ASM-SS: The First Quasi-Global High Spatial Resolution Coastal Storm Surge Dataset Reconstructed from Tide Gauge Records

Lianjun Yang[1], Taoyong Jin[1,2], and Weiping Jiang[1,2]

[1] MOE Key Laboratory of Geospace Environment and Geodesy, School of Geodesy and Geomatics, Wuhan University, Wuhan 430079, China;
[2] Hubei Luojia Laboratory, Wuhan 430079, China.

Correspondence to: Taoyong Jin (tyjin@sgg.whu.edu.cn)

Abstract. Storm surges (SSs) cause massive loss of life and property in coastal areas each year. High spatial coverage and long-term SS records are the basis for deepening our understanding of this disaster. Due to the sparse and uneven distribution of tide gauge stations, such global or quasi-global information could only be provided by global numerical models, while their simulation products span mainly the most recent decades. In this paper, for the first time, the all-site modeling framework for the data-driven model was implemented on a quasi-global scale within areas severely affected by SSs caused by tropical cyclones. Using tide gauge records and European Centre for Medium-Range Weather Forecasts Reanalysis 5 (ERA5) data, we generated a high spatial resolution (10 km along the coastline) hourly SS dataset ASM-SS (all-site modeling storm surge) within 45°S to 45°N, whose record length is over 80 years from 1940 to 2020. Assessments indicate that for 95th extreme SSs, the precision of the ASM-SS model (medians of correlation coefficients, root mean square errors, and mean biases are 0.63, 0.093 m, and -0.050 m, respectively) is better than that of the state-of-the-art global hydrodynamic model (medians are 0.55, 0.106 m, and -0.045 m); for annual maximum SSs, it is more stable than the numerical model with overall root mean square error and coefficient of determination optimizing by 22.3% and 14.8%, respectively. This dataset could provide possible alternative support for coastal communities on relevant SS analysis applications requiring high spatial resolution and sufficiently long records. The ASM-SS dataset is available at https://doi.org/10.5281/zenodo.14034726 (Yang et al., 2024a).

1 Introduction

Extreme sea level (ESL) events, defined as exceptional variations of sea-surface height caused by tides, storm surges, and sea-surface waves (Gregory et al., 2019), lead to severe economic losses globally each year (Kron, 2013). Around 680 million people living in low-lying coastal zones with elevation lower than 10 m above sea level (Pörtner et al., 2022) are already directly or indirectly affected by ESLs in current climate conditions (Hinkel et al., 2014). Even more concerning, the impacts of ESLs are expected to intensify in the future due to the rise in global sea level (Palmer et al., 2021), the increasing intensity of tropical cyclones (Knutson et al., 2020), and the growth of coastal population (Merkens et al., 2016). Storm surges (SSs) caused by tropical and extratropical cyclones have significant uncertainty compared to deterministic and predictable tides.

Understanding how SSs varied in different regions, interacted with other components, and responded to climate change in the past can better prepare coastal communities for incoming ESLs.

High-frequency (at least hourly), sufficient spatial coverage, and long-term records are important for in-depth SS analysis. To date, tide gauges (TGs) are the most reliable source of coastal sea-level observations (Marcos et al., 2019). However, their distribution is sparse and uneven. For example, as the most complete high-frequency TG collection currently, though the Global Extreme Sea Level Analysis version 3 (GESLA-3) dataset included 5,119 stations around the world, most of them were distributed in North America, Europe, Japan, and Australia (Haigh et al., 2023). Interpolating TG observations among different stations cannot accurately capture the variabilities of SSs (Muis et al., 2016) since they are affected by many factors, such as storminess, coastline shape, and bathymetry (Resio and Westerink, 2008). This always limits in-depth analysis of the spatial characteristics of SSs from TG records directly, especially on a global or quasi-global scale. In addition, though some of the oldest TG stations can date back to the eighteenth century, only ~10% (554 stations) of TG records in the GESLA-3 dataset were longer than 50 years, which makes it difficult to obtain more detailed long-term variations in SSs.

Numerical models can provide simulated data with better spatial coverage by resolving coastal physical processes inducing SSs (Muis et al., 2016, 2023; Lockwood et al., 2024). A common limitation of numerical models is that they require accurate and high-resolution bathymetric data for sufficiently precise SS estimations since SSs are significantly affected by water depth in shallow water (Resio and Westerink, 2008). However, such bathymetric data is often unavailable in nearshore areas (Cid et al., 2018). In addition, in global or quasi-global SS simulations, the coastal grid resolution of numerical models is usually set to several kilometers to balance the computational complexity (Muis et al., 2020; Mentaschi et al., 2023), which means that nearshore physical features with a spatial scale smaller than this resolution cannot be sufficiently simulated (Parker et al., 2023), and hence affecting the SS precision. Meanwhile, the computational efficiency of global numerical models tends to affect the length of simulated SSs (Muis et al., 2019). For instance, the state-of-the-art Global Tide and Surge Model (GTSM), though its outputs have been widely used in relevant studies (Kirezci et al., 2020; Dullaart et al., 2021; Fang et al., 2021; Yang et al., 2024b), its simulations spaned only the most recent decades from 1979 to 2018 (Muis et al., 2020). This imposed limitations on studies requiring long-term SS records.

Unlike numerical models, data-driven models do not need to resolve coastal physical processes. They obtain the statistical relationship between SSs (predictand) and relevant atmospheric factors (predictor) through multiple linear regression (Cid et al., 2018) or artificial intelligence (Nevo et al., 2022; Bruneau et al., 2020; Ebel et al., 2024; Nearing et al., 2024). Therefore, the precision of data-driven models is unaffected by bathymetric data and grid resolution. In addition, long-term SSs can be reconstructed efficiently after the statistical relationship is established (Tadesse et al., 2020). However, the commonly used single-site modeling framework for data-driven models heavily relies on TGs; it must establish independent relationships for every TG site by site (Cid et al., 2017; Bruneau et al., 2020; Tiggeloven et al., 2021) and cannot provide any SS information at ungauged coastal locations. For example, the Global Storm Surge Reconstruction (GSSR) database, the only publicly released global SS dataset from the data-driven model, provided SS reconstructions at 882 points globally going as far back as 1836, which benefited the research on long-term trend analysis of SSs (Tadesse and Wahl, 2021). However, it cannot address issues caused by the sparseness and uneven distribution of TG stations. Some studies replaced TG observations with numerical SS simulations to train the data-driven model (so-called 'surrogate model') (Lee et al., 2021; Ayyad et al., 2022; Lockwood et al., 2022). This combination improved the spatial resolution, but numerical models' precision limitations were also transferred to the surrogate model. Moreover, in theory, surrogate models cannot be better than numerical models compared to TG observations. Yang et al. (2023) proposed a novel all-site modeling (ASM) framework, which allowed the data-driven model to reconstruct high spatial-coverage SSs in research areas by learning from TG observations (without SS simulations from numerical models). Although single-site modeling and ASM belong to the data-driven model, their modeling processes differ. The former presumes SS observations at different TGs are independent. Therefore, the relationship between predictors and SSs needs to be learned for every TG site by site; this relationship is unsuitable for other locations. In contrast, the latter assumes there is a universal connection between SSs at different TGs, so all available TGs within the research area can be pooled into one model to learn the only relationship between predictors and SSs. This essential difference enables the ASM framework to reconstruct SSs at any coastal point in the research area. In addition, the study has shown that ASM's precision is better than single-site modeling's (Yang et al., 2023).

High spatiotemporal resolution and sufficiently long SS dataset is important for better analyzing this disaster. However, the existing SS datasets, whether from TG observations, numerical model simulations, or data-driven reconstructions, cannot fulfill all demands simultaneously on a global or quasi-global scale. The ASM provides an opportunity to fix this gap. This research used it to establish a SS data-driven model in coastal areas within ~45°S to ~45°N, which are severely affected by SSs since most destructive tropical cyclones occur here (Knapp et al., 2010). After precision assessment by comparing it with TG observations and the numerical model GTSM, we released, for the first time, a long-term (> 80 years from 1940 to 2020) quasi-global hourly SS dataset reconstructed from the data-driven model with high spatial resolution (10 km along the coastline). We hope this dataset, the ASM-SS (all-site modeling storm surge), can provide possible alternative support for coastal communities to deepen the understanding of SSs and ESLs.

2 Materials and Methods

2.1 Atmospheric Data

Atmospheric predictors from 1940 to 2020 were obtained from the European Centre for Medium-Range Weather Forecasts (ECMWF) Reanalysis v5 (ERA5) database (Soci et al., 2024). It is the fifth generation ECMWF reanalysis through assimilating model data with observations across the world into a globally complete and consistent dataset, which can provide hourly atmosphere fields with a 0.25°×0.25° resolution grid. Following Yang et al.(2023) and Yang et al.(2024b), four variables from ERA5 were used, including mean sea level pressure (mslp), 10 m eastward and northward wind (u10, v10), and 2 m temperature (t2m).

2.2 Tide Gauge Data

TG observations from 1940 to 2020 came from the high-frequency (15 minutes or one hour) GESLA-3 dataset collected from 36 international and national data providers (Haigh et al., 2023). This dataset unified the time units (to coordinated universal time) and length units (to meters) of water level records from different sources. In addition, the analysis flag was added to each TG record, making it convenient to select available sea-level data. However, a stricter quality control process is needed since some sites still contain datum jumps and outliers (Haigh et al., 2023). Detailed TG preprocessing is as follows:

(1) Coastal TG stations located between 45°S-45°N were selected (excluding the Mediterranean, Black, and Caspian Sea). Additionally, two stations at the southernmost tip of New Zealand were retained, though they are beyond 45°S;

(2) For the case that TG data was provided by different sources covering similar periods, the file with longer records was kept; for the case that the sea-level time series for the same site was split into different files, they were merged to obtain the longest possible records;

(3) TG data were resampled to hourly, and the analysis flag=1 (means 'use') was used to filter out the available data for each TG. Datum jumps caused by earthquakes or changes in instrument were adjusted, and obvious outliers were removed through visual inspection. Then, 1,315 stations with a length longer than one year remained (Fig. 1);

(4) After removing the inter-annual mean sea-level variability from TG data through the annual moving average, the SS time series can be obtained by subtracting tides estimated from the Utide (Unified Tidal Analysis and Prediction Functions) package (Codiga, 2011), which can select the most important components from 146 tidal constituents through an automated decision tree;

(5) Finally, a 12-hour moving average was applied to SS data to limit possible remaining tidal signals (Tiggeloven et al., 2021; Yang et al., 2023), which are generally generated by small phase shifts in predicted tides due to the difficulty of obtaining perfect and completely accurate estimates through harmonic analysis (Horsburgh and Wilson, 2007).

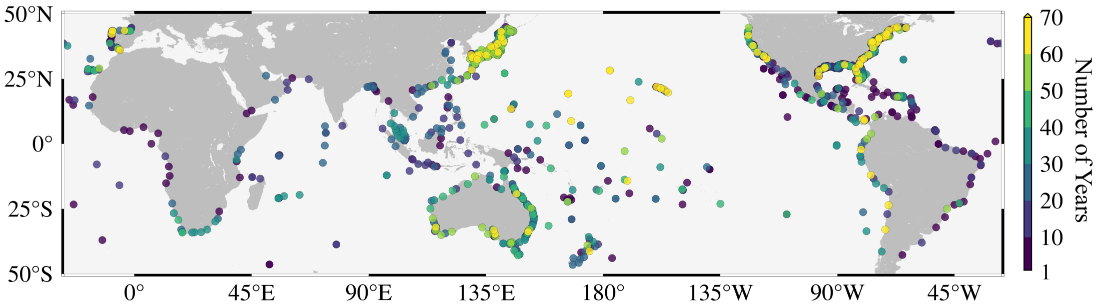

Figure 1: The distribution and data length of selected tide gauges.

2.3 Surge Data Simulated from Numerical Model

Numerical model SSs came from GTSM version 3 global simulation forced with mean sea level pressure and wind from the ERA5 reanalysis (1979-2018), whose SS precision has been extensively evaluated and shown to have fair to good agreement with TG observations (Bloemendaal et al., 2019; Muis et al., 2020; Parker et al., 2023; Yang et al., 2023). This model was solved based on Delft3D Flexible Mesh (Kernkamp et al., 2011) with the unstructured grid resolution from 2.5 km (1.25 km in Europe) along the coast to 25 km in the deep ocean (Muis et al., 2020). It provided outputs both in the ocean and along the coastline; the latter's resolution was resampled to approximately every 20 km per coastal point to limit the data volume (Muis et al., 2020). Note that GTSM SSs were only used to assess our ASM data-driven model; they were not used in the training process of the latter.

2.4 Coastline Contour Data

The Global Self-consistent, Hierarchical, High-resolution Geography (GSHHG version 2.3.7) shoreline database (Wessel and Smith, 1996) was used to generate coastal nodes for the ASM-SS in the research area (45°S to 45°N). The shoreline of this dataset was developed from the World Vector Shorelines and Atlas of the Cryosphere, providing five different-resolution coastline contours (crude, low, intermediate, high, and full). We used the high-resolution data (~300m). After smoothing the shoreline with a window of 50 points, coastal nodes with a 10 km resolution were sampled evenly from the smoothed coastline. Figure 2 shows their distribution. The total number of nodes is 20,440: Western Europe (200), Africa (2,806), North America (3,165), South America (2,218), Oceania (3,471), and Asia (8,580).

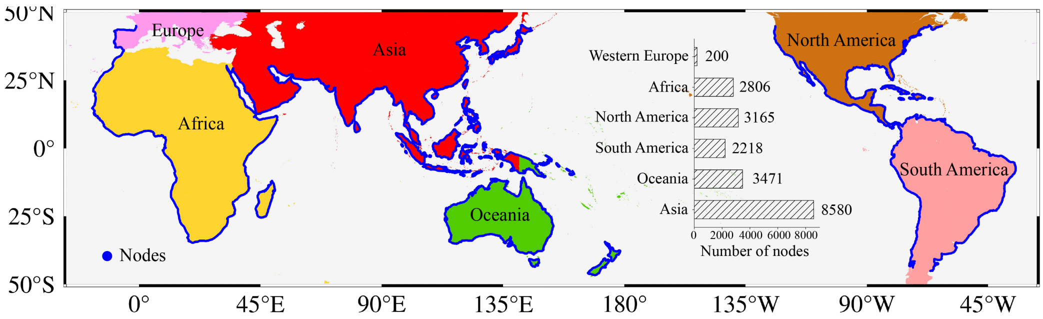

Figure 2: The distribution of coastal nodes for reconstructed storm surges.

2.5 All-site Modeling Framework

Full details of the ASM can be found at Yang et al.(2023). Here, a brief description of its modeling processes is provided. Assuming there are six available TGs within 45°S to 45°N (Fig. 3(a)):

(1) Obtaining predictors (Fig. 3(b)). Four atmospheric data (mslp, u10, v10, and t2m) for each TG station are extracted from the ERA5 dataset through linear interpolation. Changes in sea level pressure and wind are the main factors in generating SSs (Woodworth et al., 2019); adding temperature variations considers the effects of thermal expansion and contraction. Meanwhile, following Yang et al.(2023) and Yang et al.(2024b), another three variables (longitude, latitude, and timestamp) are considered since geographical locations and record lengths of TGs are different. Hence, the predictor matrix for each TG consists of 7 columns: mslp, u10, v10, t2m, longitude, latitude, and time;

(2) All-site modeling (Fig. 3(c)). Predictor matrices and SSs of all six TG stations are stacked into one predictor matrix and one SS matrix. Then, the eXtreme Gradient Boosting Tree (XGBoost) (Chen & Guestrin, 2016) is used to learn the relationship

between these two matrices. The XGBoost is a residual machine learning model that generates a new decision tree using SS residuals from the previous tree. Therefore, the new tree will pay more attention to training where the residual errors are significant, making it suitable for modeling SS extremes;

(3) Reconstruction (Fig. 3(d)). SSs can be estimated for any target node along the coastline by inputting the corresponding predictor matrix of that location into the model established in step (2).

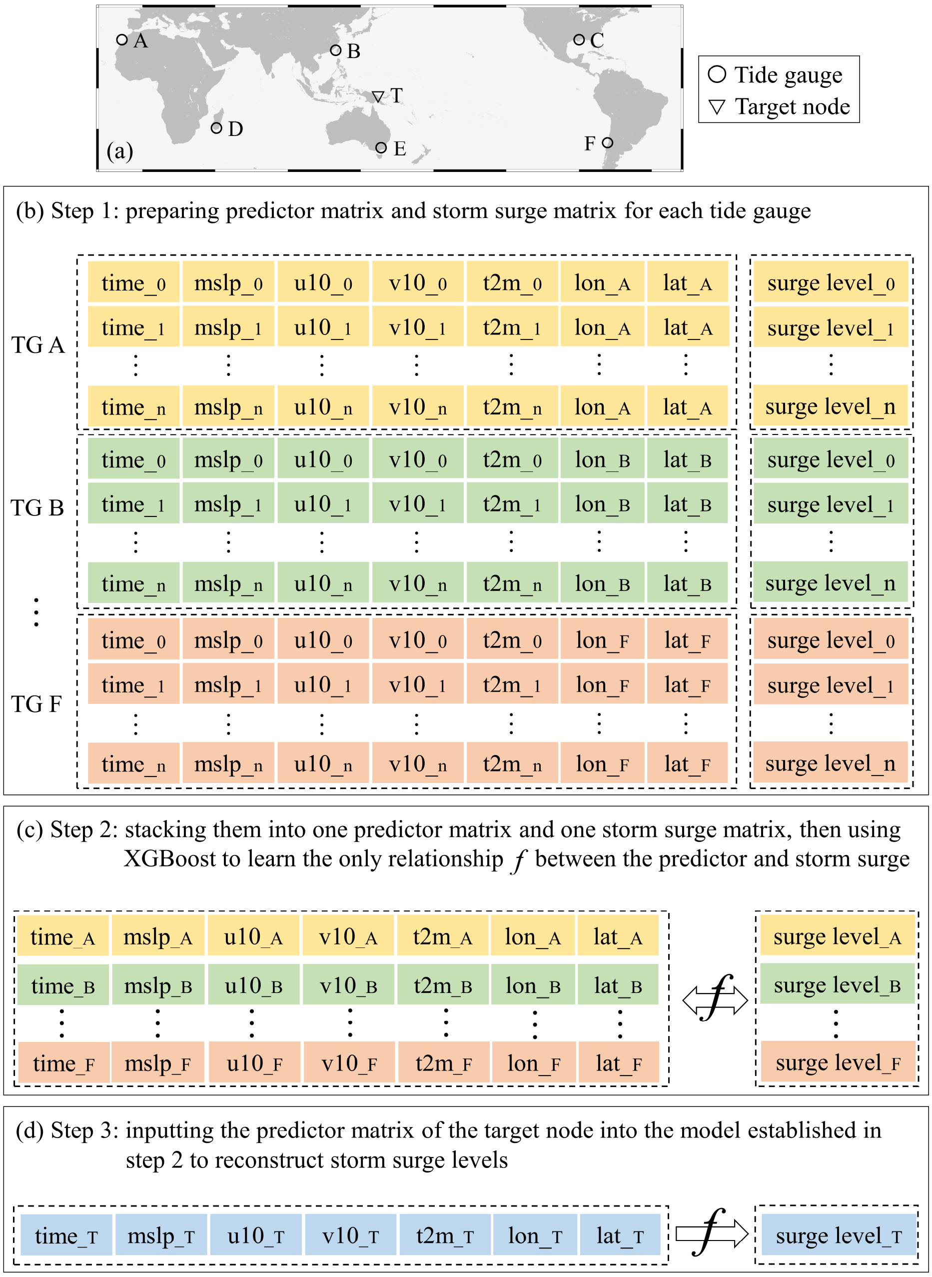

Figure 3: The modeling processes of the ASM framework

2.6 Model Performance Metrics

Three model performance metrics are used to evaluate the differences between reconstructed and observed SS levels: Pearson product-moment correlation coefficient (CORR), root mean square error (RMSE), and mean bias (MB):

$$\mathrm{CORR}=\frac{\sum_{i=1}^{N}\left(\mathrm{SSL}_{r,i}-\overline{\mathrm{SSL}_r}\right)\left(\mathrm{SSL}_{o,i}-\overline{\mathrm{SSL}_o}\right)}{\sqrt{\sum_{i=1}^{N}\left(\mathrm{SSL}_{r,i}-\overline{\mathrm{SSL}_r}\right)^2}\sqrt{\sum_{i=1}^{N}\left(\mathrm{SSL}_{o,i}-\overline{\mathrm{SSL}_o}\right)^2}} \tag{1}$$

$$\mathrm{RMSE}=\sqrt{\frac{\sum_{i=1}^{N}\left(\mathrm{SSL}_{r,i}-\mathrm{SSL}_{o,i}\right)^2}{N}} \tag{2}$$

$$\mathrm{MB}=\frac{1}{N}\sum_{i=1}^{N}\left(\mathrm{SSL}_r-\mathrm{SSL}_o\right) \tag{3}$$

where N is the length of the evaluation time series; $\mathrm{SSL}_{r,i}$ and $\mathrm{SSL}_{o,i}$ indicate the reconstructed and observed SS levels, respectively. $\overline{\mathrm{SSL}_r}$ and $\overline{\mathrm{SSL}_o}$ are the average values of them.

3 Results

3.1 ASM Model Evaluation at Tide Gauges

The k-fold cross-validation strategy was chosen to evaluate the ASM model at TGs. 823 TG stations with time lengths exceeding 10 years between 1940 and 2020 were randomly divided into ten parts (i.e., 10-fold cross-validation), with the last part containing 85 TGs. Each time, 9 of the parts were used for training. After the model was established, predictor matrices of the excluded part of TGs were inputted into the model to obtain their SSs. The SSs of all parts of TGs can be estimated once each part has been excluded. Then, we compared the reconstructed entire surge time series (evaluating the overall variation trend) and the 95th percentile SSs (assessing extreme events) with TG observations. As shown in Fig. 4 and Table 1, we divided the research area into fifteen sub-regions (ER: the equatorial region, WEU: Western Europe, NAF: Northern Africa, SWA: Southwestern Africa, SEA: Southeastern Africa, WNA: Western North America, ENA: Eastern North America, CA: Central America, SWS: Southwestern South America, SES: Southeastern South America, WAS: Western Asia, EAS: Eastern Asia, SAS: Southern Asia, NOC: Northern Oceania, and SOC: Southern Oceania) for more detailed assessment information. Note that the equatorial region (~6°S to ~6°N) was separated as an independent area since it has almost no tropical cyclones.

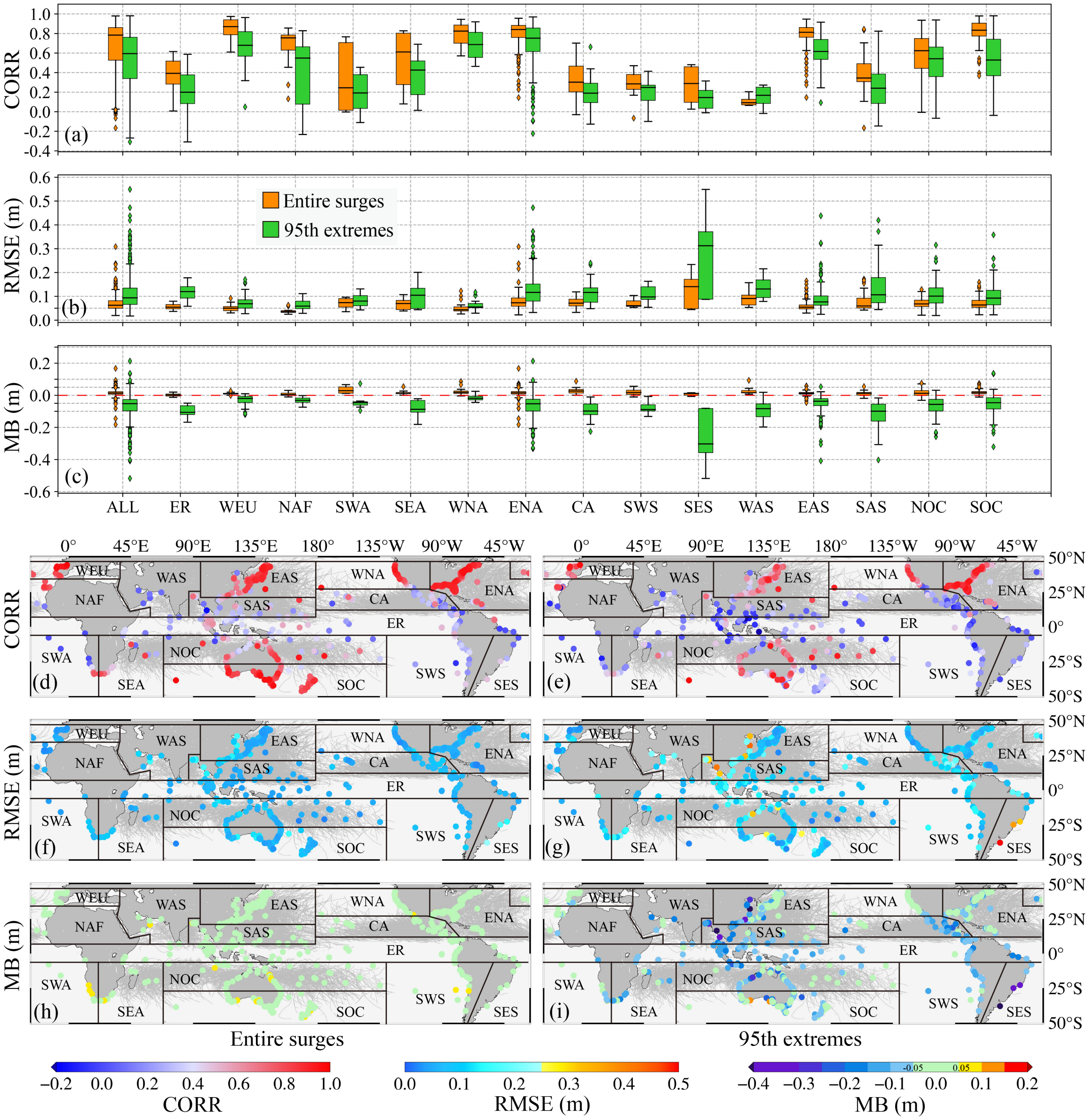

175

Figure 4: ASM model evaluation at tide gauges from 1940 to 2020. (a-c) Entire surge and 95th extreme evaluation statistics for different regions; (d-i) Distributions of evaluation metrics. Gray lines are tropical cyclone paths.

Table 1: The median of evaluation statistics for different regions in Fig. 4.

	Median of CORRs		Median of RMSEs (m)		Median of MBs (m)	
	Entire surges	95th extremes	Entire surges	95th extremes	Entire surges	95th extremes
ALL	0.78	0.59	0.063	0.094	0.014	-0.052
ER	0.39	0.20	0.054	0.120	0.002	-0.106
WEU	0.87	0.68	0.050	0.069	0.011	-0.020
NAF	0.76	0.55	0.036	0.059	0.004	-0.031
SWA	0.25	0.19	0.074	0.080	0.029	-0.046
SEA	0.61	0.43	0.070	0.105	0.012	-0.087
WNA	0.83	0.69	0.044	0.055	0.018	-0.019
ENA	0.84	0.75	0.073	0.117	0.016	-0.053
CA	0.30	0.19	0.072	0.116	0.027	-0.098
SWS	0.29	0.25	0.061	0.098	0.017	-0.088
SES	0.29	0.15	0.141	0.312	0.011	-0.303
WAS	0.09	0.17	0.091	0.131	0.016	-0.083
EAS	0.81	0.62	0.054	0.077	0.013	-0.037
SAS	0.34	0.24	0.060	0.107	0.012	-0.099
NOC	0.62	0.54	0.068	0.101	0.013	-0.056
SOC	0.83	0.53	0.064	0.093	0.017	-0.046

Figure 4(a-c) and Table 1 show that on a quasi-global scale (i.e., for ALL TGs), the median CORR of the entire time series of surges is 0.78, RMSE is 0.063m, and MB is 0.014m. In comparison, the reconstruction precision for extreme events (>95th percentile) is lower: CORR is 0.59, RMSE is 0.094m, and MB is -0.052m (indicating a slight underestimation of the magnitude of extreme events). At the regional scale, there are differences between sub-regions (Fig. 4(d-i)). In areas with almost no tropical cyclones, including ER, SWA, SWS, and SES, precision is low for both entire surges and 95th extremes. For other places, the precision of estimated SSs is better in regions with a relatively high density of TG stations, such as WEU, WNA, ENA, EAS, NOC, and SOC. This result is consistent with the conclusion of Yang et al. (2024b) that reducing the spatial interval of TG stations can benefit the estimation of SSs, especially the extremes.

It is necessary to evaluate temporal variations in reconstructed SSs further since their length is over 80 years, during which the number of TG stations and the quality of atmospheric data have changed. As shown in Fig. 5, the precision of ASM model at TGs in each sub-region was calculated every 10 years (excluding TGs with less than one year of data in a given decade). Results indicate that the overall precision (i.e., for ALL TGs) of entire surges and 95th extremes gradually increased from 1940 to 2020. Possible reasons are as follows: on the one hand, ASM model is affected by the spatial resolution of TGs (Yang et al., 2024b). The increase of TGs in recent decades (Haigh et al., 2023) enhances its precision; on the other hand, the quality of ERA5 reanalysis data improved as increasing satellite data has been assimilated since the 1970s (Soci et al., 2024), which benefits the data-driven model. At the regional scale, for entire surges, Figure 5(a) indicates that except for SWA (CORR decreases) and WAS (CORR remains unchanged), CORRs of other sub-regions present an upward trend; Figure 5(b) shows the RMSE in SES increases, while RMSEs in other regions decrease; Figure 5(c) gives that MBs of sub-regions have been gradually optimized (excluding WAS). For 95th extremes, in terms of CORR (Fig. 5(d)), WEU, NAF, WNA, ENA, EAS, NOC, and SOC show an upward trend, whereas there is no obvious pattern in other regions; for RMSE (Fig. 5(e)), ER, SEA, and SES present an increasing trend, other regions decrease; for MB (Fig. 5(f)), the underestimation of SSs in ER and SAS rises, and there is no noticeable change in WNA and SES. MBs in WEU, NAF, ENA, WAS, EAS, NOC, and SOC are optimized, while there is no clear pattern in SWA, SEA, CA, and SWS.

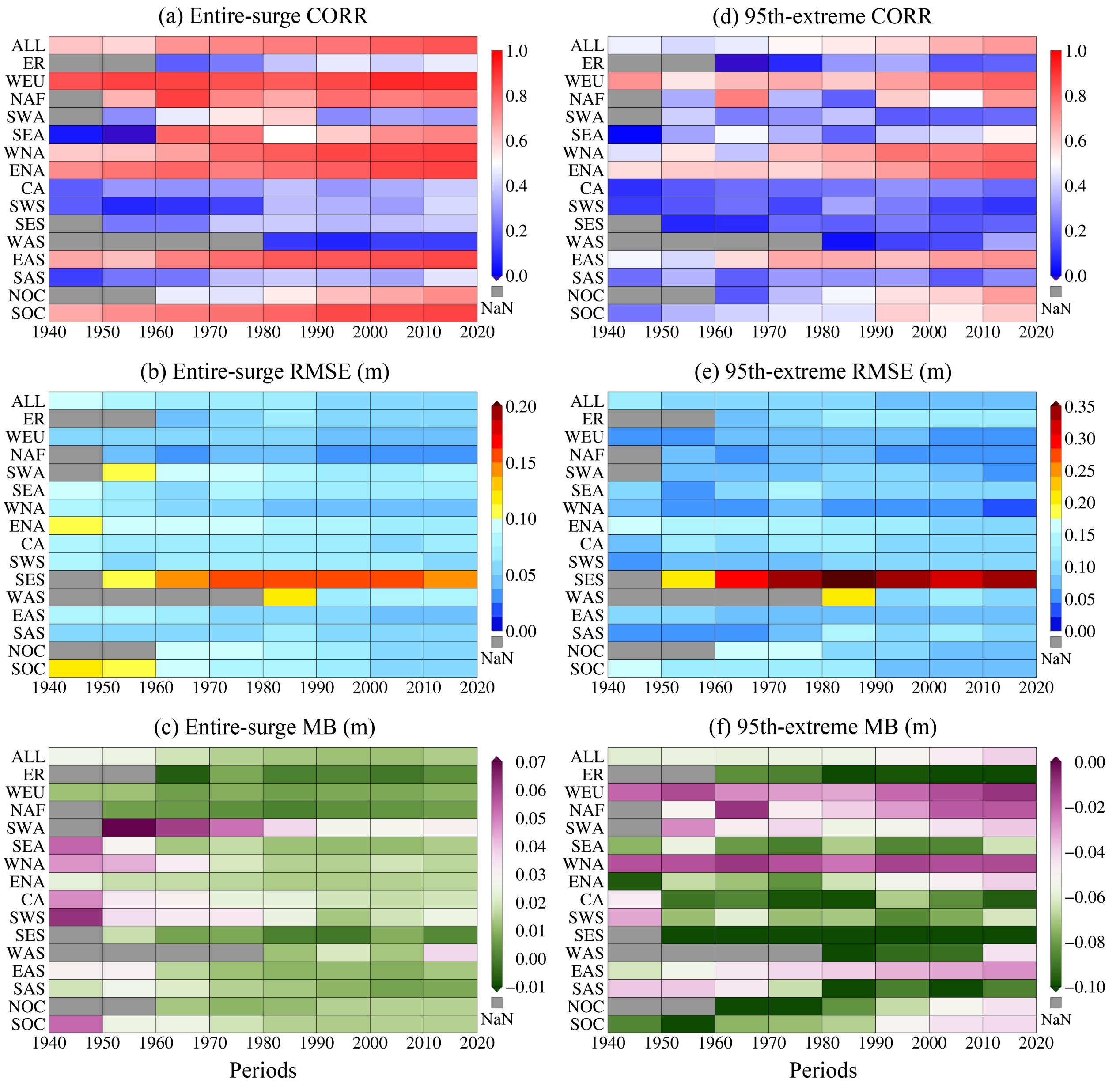

Figure 5: Temporal variations of the ASM model's precision at tide gauges from 1940 to 2020. (a-c) Entire surge evaluation statistics for different regions every 10 years; (d-f) 95th extreme evaluation statistics for different regions every 10 years

3.2 ASM Model Comparison with Numerical Model at Tide Gauge Scale

Since GTSM provided numerical surges from 1979 to 2018, ASM data in the same period were extracted from SSs reconstructed in section 3.1. In addition, since points of GTSM did not completely coincide with TG stations, linear interpolation was used to interpolate GTSM SSs to corresponding TG locations. Figure 6 and Table 2 give the 95th extremes comparison results between ASM, GTSM, and TG observations.

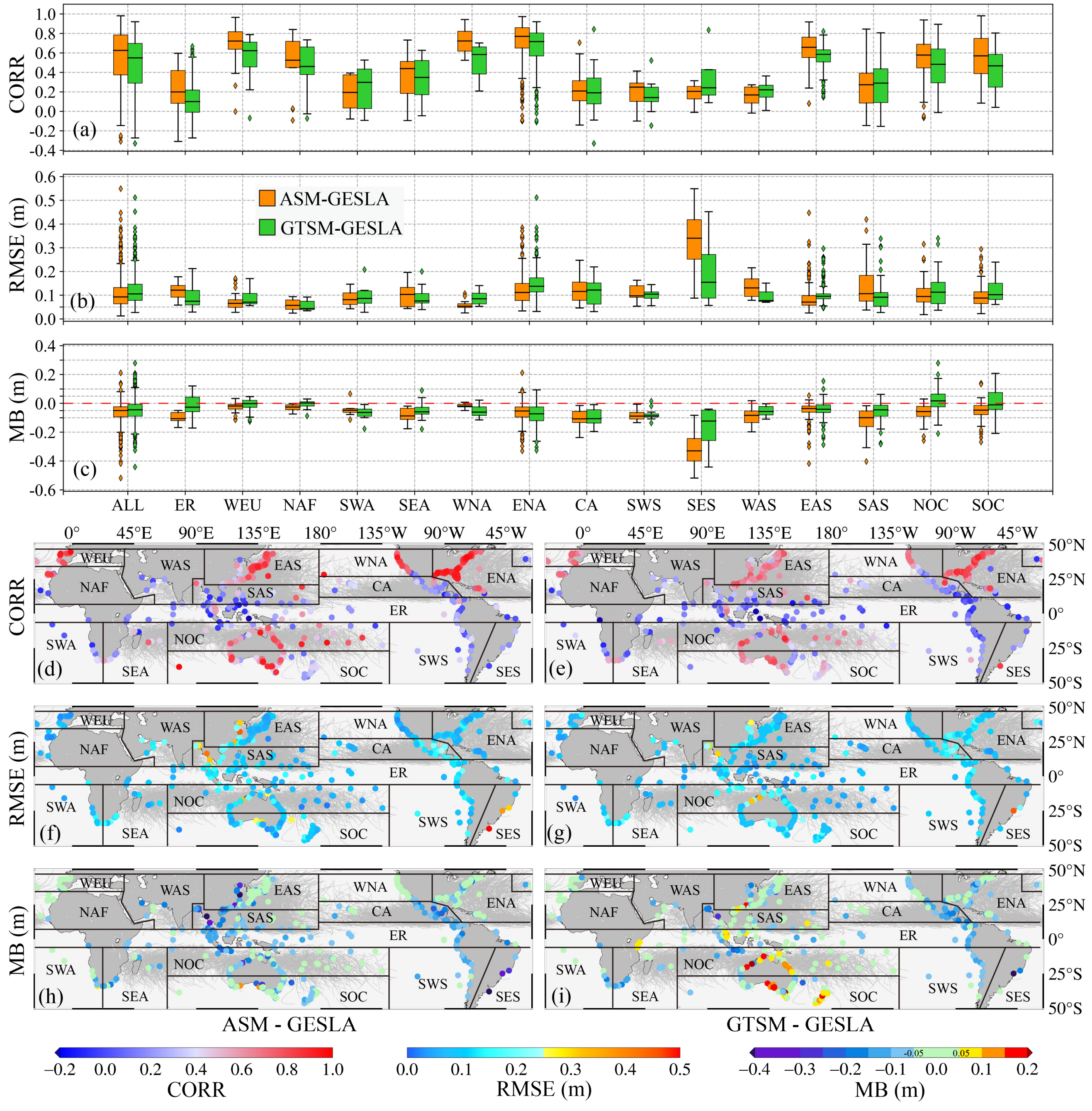

Figure 6: ASM model comparison with the numerical model at tide gauges from 1979 to 2018. (a-c) ASM and GTSM 95th extreme evaluation statistics for different regions; (d-i) Distributions of evaluation metrics. Gray lines are tropical cyclone paths.

Table 2: The median of evaluation statistics for different regions in Fig. 6.

	Median of CORRs	Median of RMSEs (m)	Median of MBs (m)

	ASM-GESLA	GTSM-GESLA	ASM-GESLA	GTSM-GESLA	ASM-GESLA	GTSM-GESLA
ALL	0.63	0.55	0.093	0.106	-0.050	-0.045
ER	0.20	0.10	0.122	0.075	-0.106	-0.026
WEU	0.72	0.62	0.066	0.071	-0.019	-0.001
NAF	0.53	0.46	0.057	0.044	-0.025	0.003
SWA	0.20	0.30	0.081	0.087	-0.048	-0.063
SEA	0.44	0.35	0.103	0.076	-0.087	-0.058
WNA	0.72	0.58	0.054	0.085	-0.019	-0.061
ENA	0.77	0.72	0.112	0.138	-0.052	-0.072
CA	0.21	0.19	0.116	0.122	-0.107	-0.106
SWS	0.25	0.14	0.098	0.105	-0.088	-0.086
SES	0.21	0.24	0.340	0.155	-0.329	-0.123
WAS	0.17	0.22	0.131	0.077	-0.083	-0.056
EAS	0.66	0.59	0.071	0.096	-0.036	-0.041
SAS	0.27	0.29	0.107	0.092	-0.099	-0.045
NOC	0.58	0.48	0.095	0.113	-0.057	0.017
SOC	0.57	0.47	0.088	0.102	-0.047	-0.010

It can be seen from Fig. 6(a-c) and Table 2 that on the quasi-global scale, ASM (medians of CORRs, RMSEs, and MBs for 95th extremes are 0.63, 0.093 m, and -0.050 m, respectively) outperforms the numerical model GTSM (medians are 0.55, 0.106 m, and -0.045 m). At the regional scale (Fig. 6(d-i)), ASM and GTSM perform poorly in areas with no tropical cyclones (ER, SWA, SWS, and SES), indicating that in addition to meteorological factors, oceanographic processes in these regions also contribute to the extremes (Cid et al., 2017; Woodworth et al., 2019). For areas severely affected by tropical cyclones (such as WEU, WNA, ENA, EAS, NOC, and SOC), ASM and GTSM are more precise. Moreover, CORRs and RMSEs of ASM are better than those of GTSM in these sub-regions, while MBs of GTSM are closer to zero meter in WEU, NOC, and SOC (Fig. 6(a-c)). However, GTSM appears to overestimate extremes in some areas, such as NOC and SOC (Fig. 6(i)). For further insight, Figure 7 presents scatter density plots of ASM and GTSM annual maximum SSs compared with TG records. Among the fifteen sub-regions, the determination coefficient (R^2) of ASM in 10 of them is better than GTSM (Fig. 7(b-i, k, o)); the RMSE of ASM is smaller than GTSM in 12 areas (Fig. 7(b-j, m, o, p)). However, there are two sub-regions where the R^2 and RMSE of ASM are worse than that of GTSM ((Fig. 7(l, n)), possibly because the available TGs are sparse, especially in WAS. On a quasi-global scale, ASM's overall RMSE and R^2 improvements compared to GTSM are 22.3% (from 0.184 m to 0.143 m) and 14.8% (from 0.61 to 0.70), respectively (Fig. 7(a)), which means ASM is more stable than GTSM. The reason why ASM outperforms GTSM can be attributed to two main aspects. For the global numerical model GTSM, as mentioned in the introduction, the accuracy and spatial resolution of bathymetric data in the nearshore area limits the precision of SSs. Meanwhile, the grid with a resolution of several kilometers affects the effective simulation of small-scale physical factors. For the ASM data-driven model, the training process is based on TG observations. TGs are the most accurate source for sea level monitoring, and their records can be considered to include effects from all spatial-scale physical processes. In addition, the machine learning method XGBoost is a residual model that pays more attention to where residual errors are significant, which also benefits the estimation of extreme SSs.

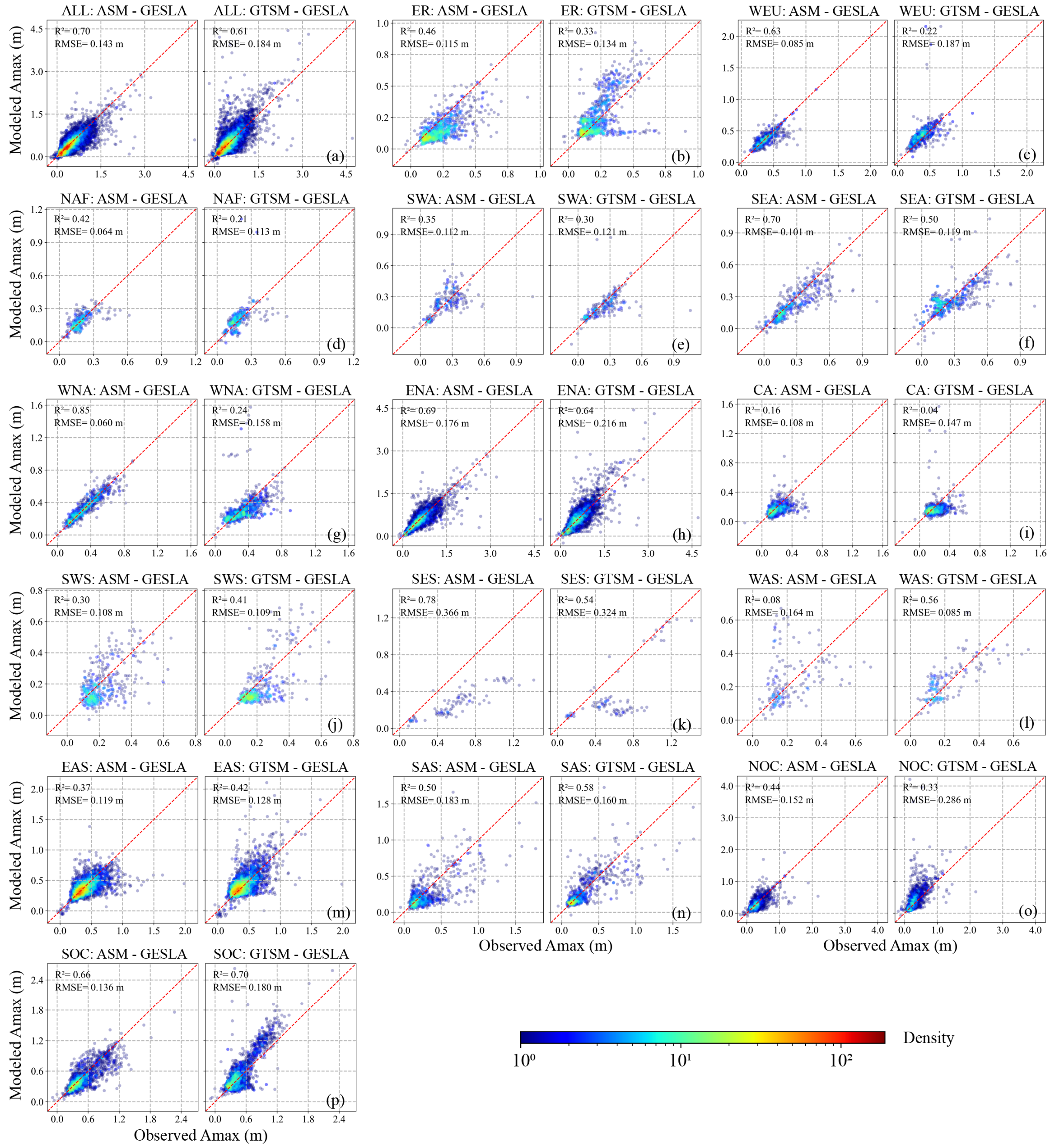

Figure 7: Scatter density plots of ASM and GTSM annual maxima (Amax) compared with tide gauge observations in different regions. The data for tide gauges were combined. The red dotted line indicates the perfect fit line.

3.3 ASM Model Comparison with Numerical Model at Coastal Scale

As mentioned in the introduction, though ASM and single-site modeling belong to the data-driven model, the former can provide SS information for ungauged points since their basic ideas differ. This advantage of ASM allows us to compare the data-driven model and numerical model on a quasi-global scale with high spatial resolution. In this section, the ASM model was trained based on all 1,315 TGs within the research area with records longer than one year from 1940 to 2020 (Figure 1). Then SSs from 1979 to 2018 were reconstructed to all coastal points of GTSM to assess their differences (Fig. 8 and Table 3).

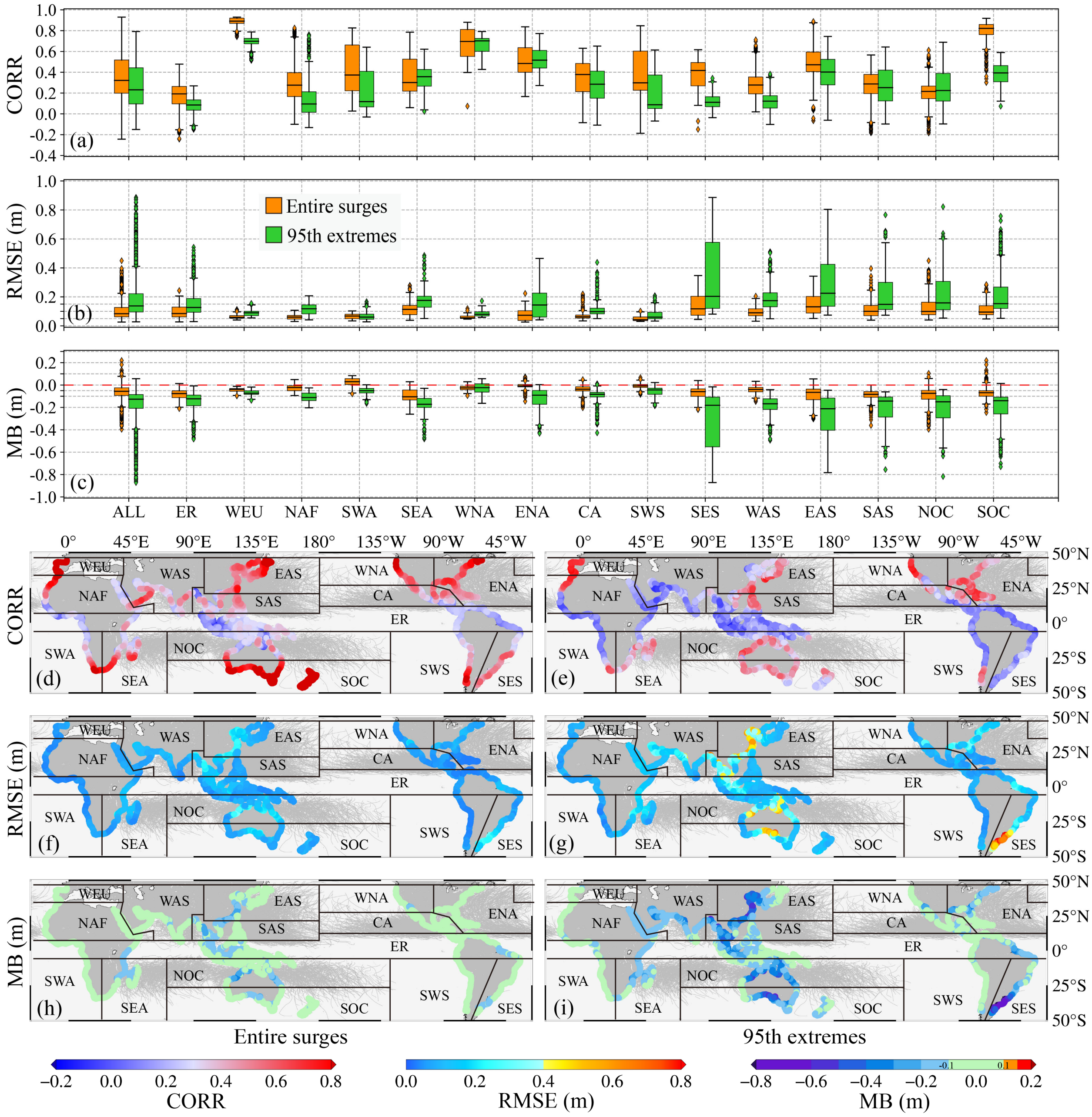

245 **Figure 8: Differences between ASM and GTSM at the coastal scale from 1979 to 2018. (a-c) Comparison statistics between ASM and GTSM modeled entire surges and 95th extremes for different regions; (d-i) Distributions of comparison metrics. Gray lines are tropical cyclone paths.**

Table 3: The median of evaluation statistics for different regions in Fig. 8.

	Median of CORRs		Median of RMSEs (m)		Median of MBs (m)	
	Entire surges	95th extremes	Entire surges	95th extremes	Entire surges	95th extremes
ALL	0.32	0.23	0.084	0.138	-0.056	-0.126
ER	0.19	0.09	0.085	0.127	-0.076	-0.123
WEU	0.89	0.70	0.058	0.090	-0.039	-0.073
NAF	0.28	0.10	0.060	0.118	-0.022	-0.112
SWA	0.37	0.12	0.068	0.060	0.030	-0.050
SEA	0.30	0.36	0.114	0.176	-0.105	-0.172
WNA	0.70	0.70	0.055	0.080	-0.025	-0.023
ENA	0.48	0.52	0.073	0.144	-0.009	-0.091
CA	0.38	0.28	0.063	0.098	-0.037	-0.083
SWS	0.30	0.09	0.043	0.060	-0.008	-0.044
SES	0.42	0.11	0.118	0.204	-0.059	-0.180
WAS	0.28	0.12	0.090	0.174	-0.040	-0.167
EAS	0.47	0.40	0.132	0.225	-0.065	-0.212
SAS	0.29	0.25	0.100	0.148	-0.083	-0.143
NOC	0.22	0.22	0.100	0.159	-0.074	-0.149
SOC	0.82	0.39	0.095	0.154	-0.068	-0.140

Figure 8 and Table 3 give the comparison results between ASM and GTSM modeled entire surges and 95th extremes. Note that since both ASM and GTSM SSs were estimated, we used GTSM as the baseline here. As shown in Fig. 8 and Table 3, there are noticeable differences between ASM and GTSM. On the quasi-global scale, medians of CORRs, RMSEs, and MBs of the entire surges (95th extremes) between them are 0.32 (0.23), 0.084 m (0.138 m), and -0.056 m (-0.126 m), respectively (Fig. 8(a-c)). The negative MBs indicate that ASM tends to give lower SS estimates than GTSM, which is consistent with the conclusion from the comparison with TGs in section 3.2. From the regional perspective, the agreement between ASM and GTSM (Fig. 8(d, f, h) for entire surges, Fig. 8(e, g, i) for 95th extremes) are better in WEU, SEA, WNA, ENA, EAS and SOC. For other places, on the one hand, both ASM and GTSM showed relatively poor agreement with TG observations in section 3.2 (Fig. 6 (d-i)); on the other hand, there are also visible discrepancies between ASM and GTSM (Fig. 8(d-i)). Possible reasons could be as follows: For ASM, its extreme SS reconstruction is affected by the distribution and spatial interval of TG stations (Yang et al., 2024b). For GTSM, the grid resolution and the bathymetric data's precision also impact the simulation results. Additionally, neither of them considers sea level variations caused by runoff and precipitation. Nevertheless, the precision of ASM and GTSM for these regions needs further improvement in the future.

4 Data availability

The ASM-SS quasi-global storm surge dataset was generated from the ASM data-driven model established in section 3.3. The dataset is available at https://doi.org/10.5281/zenodo.14034726 (Yang et al., 2024a) as NetCDF files month by month from 1940 to 2020. Each file includes five parameters: longitude, latitude, nodes, time, and surge level. Longitude and latitude are the location information of nodes in degree; the unit of time is accumulated hours since 1900-01-01 00:00:00; surge levels are given in meters. Users can use longitude, latitude, and time as keywords to select surge levels at nodes of interest within a target period. In addition, the spatial resolution of nodes is 10 km along the coastline (as shown in Figure 2). Since the sea surface varies rapidly during tropical cyclones, the temporal resolution of surge levels is set to hourly. Though this temporal resolution increases the data volume, it can provide sufficient information for users who want to analyze high-frequency variations of storm surges during extreme events.

5 Conclusion and Discussion

High spatial coverage and long-term SS records are the basis for deepening our understanding and better preparing coastal communities for incoming ESLs. However, high spatial resolution SS information on a global or quasi-global scale could only be simulated by global numerical models due to the sparse and uneven distribution of TG stations. Here, based on the ASM framework, we established a SS data-driven model using observations from TGs between 45°S-45°N. Then, for the first time, a high spatial resolution (every 10 km per node along the coastline), long-term (over 80 years from 1940 to 2020), quasi-global (within 45°S-45°N), hourly data-driven SS dataset ASM-SS was reconstructed from this ASM model. Evaluation results indicate that for 95th extreme SSs, this model (medians of CORRs, RMSEs, and MBs are 0.63, 0.093 m, and -0.050 m, respectively) is better than the state-of-the-art hydrodynamic model GTSM (medians are 0.55, 0.106 m, and -0.045 m); for annual maximum SSs, ASM is more stable than GTSM with overall RMSE and coefficient of determination optimizing by 22.3% and 14.8%, respectively. This dataset could provide possible alternative support aside from numerical models for coastal communities to analyze variations of SSs, assess the contribution of SSs to ESL, and other relevant applications.

Nonetheless, several details of this model can be studied more deeply in our future work: (1) Generally speaking, tropical cyclones are usually accompanied by heavy rainfall when they make landfall, which might affect sea-surface height. In addition, the impact of river runoff in estuarine areas may need to be considered. (2) The distribution and spatial interval of TG stations have been proven to affect the precision of ASM (Yang et al., 2024b). Because establishing and maintaining a permanent TG network with high spatial coverage in coastal regions is expensive and complex, it is necessary to consider integrating various water level observation technologies, such as Global Navigation Satellite System reflectometry (GNSS-R) and satellite altimetry. (3) From the predictor side, several studies showed that ERA5 data tends to relatively underestimate higher wind speeds (Graham et al., 2019; Xiong, 2022), which may lead to underestimations of extreme SSs. Therefore, the atmospheric predictors can also be optimized through multi-source data fusion, such as considering wind speeds obtained from spaceborne GNSS-R (e.g., Cyclone Global Navigation Satellite System) or cyclone information obtained from remote sensing satellites.

Author contribution. LY and TJ designed the research. LY carried out the experimental results and wrote the initial manuscript. TJ and WJ provided related comments for this work and revised the manuscript.

Competing interests. The authors declare that they have no conflict of interest.

Acknowledgments. The authors are very grateful to the Climate Data Store for providing ERA5 (Copernicus Climate Change Service, 2018) and GTSM data (Copernicus Climate Change Service, 2022). We would also like to thank the publication of the GESLA-3 dataset, which helps us save much time in tide gauge collection and data preprocessing. (https://gesla787883612.wordpress.com, last access: 28 March 2025). The shoreline database GSSHS version 2.3.7 is available online (https://www.ngdc.noaa.gov/mgg/shorelines, last access: 28 March 2025). The tropical cyclone paths shown in Fig. 4, 6, and 8 are from Gahtan et al. (2024). All the respectable reviewers and editors are acknowledged for their professional suggestions for this paper.

Financial support. This research was funded by the National Natural Science Foundation of China under Grants 42374035, 42192531, and 42388102, and the Fundamental Research Funds for the Central Universities.

References

Ayyad, M., Hajj, M. R., and Marsooli, R.: Machine learning-based assessment of storm surge in the New York metropolitan area, Sci Rep, 12, 19215, https://doi.org/10.1038/s41598-022-23627-6, 2022.

Bloemendaal, N., Muis, S., Haarsma, R. J., Verlaan, M., Irazoqui Apecechea, M., De Moel, H., Ward, P. J., and Aerts, J. C. J. H.: Global modeling of tropical cyclone storm surges using high-resolution forecasts, Clim Dyn, 52, 5031–5044, https://doi.org/10.1007/s00382-018-4430-x, 2019.

Bruneau, N., Polton, J., Williams, J., and Holt, J.: Estimation of global coastal sea level extremes using neural networks, Environ. Res. Lett., 15, 074030, https://doi.org/10.1088/1748-9326/ab89d6, 2020.

Chen, T. and Guestrin, C.: XGBoost: A Scalable Tree Boosting System, in: Proceedings of the 22nd ACM SIGKDD International Conference on Knowledge Discovery and Data Mining, arXiv:1603.02754 [cs], 785–794, https://doi.org/10.1145/2939672.2939785, 2016.

Cid, A., Camus, P., Castanedo, S., Méndez, F. J., and Medina, R.: Global reconstructed daily surge levels from the 20th Century Reanalysis (1871–2010), Global and Planetary Change, 148, 9–21, https://doi.org/10.1016/j.gloplacha.2016.11.006, 2017.

Cid, A., Wahl, T., Chambers, D. P., and Muis, S.: Storm Surge Reconstruction and Return Water Level Estimation in Southeast Asia for the 20th Century, JGR Oceans, 123, 437–451, https://doi.org/10.1002/2017JC013143, 2018.

Codiga, D. L.: Unified Tidal Analysis and Prediction Using the UTide Matlab Functions, 2011.

Copernicus Climate Change Service: ERA5 hourly data on single levels from 1940 to present [data set], https://doi.org/10.24381/cds.adbb2d47, 2018.

Copernicus Climate Change Service: Global sea level change time series from 1950 to 2050 derived from reanalysis and high resolution CMIP6 climate projections [data set], https://doi.org/10.24381/cds.a6d42d60, 2022.

Dullaart, J. C. M., Muis, S., Bloemendaal, N., Chertova, M. V., Couasnon, A., and Aerts, J. C. J. H.: Accounting for tropical cyclones more than doubles the global population exposed to low-probability coastal flooding, Commun Earth Environ, 2, 135, https://doi.org/10.1038/s43247-021-00204-9, 2021.

Ebel, P., Victor, B., Naylor, P., Meoni, G., Serva, F., and Schneider, R.: Implicit Assimilation of Sparse In Situ Data for Dense & Global Storm Surge Forecasting, in: 2024 IEEE/CVF Conference on Computer Vision and Pattern Recognition Workshops (CVPRW), 2024 IEEE/CVF Conference on Computer Vision and Pattern Recognition Workshops (CVPRW), Seattle, WA, USA, 471–480, https://doi.org/10.1109/CVPRW63382.2024.00052, 2024.

Fang, J., Wahl, T., Zhang, Q., Muis, S., Hu, P., Fang, J., Du, S., Dou, T., and Shi, P.: Extreme sea levels along coastal China: uncertainties and implications, Stoch Environ Res Risk Assess, 35, 405–418, https://doi.org/10.1007/s00477-020-01964-0, 2021.

Gahtan, J., Knapp, K. R., Schreck, C. J. I., Diamond, H. J., Kossin, J. P., and Kruk, M. C.: International Best Track Archive for Climate Stewardship (IBTrACS) Project, Version 4.01 [data set], https://doi.org/10.25921/82ty-9e16, 2024.

Graham, R. M., Hudson, S. R., and Maturilli, M.: Improved Performance of ERA5 in Arctic Gateway Relative to Four Global Atmospheric Reanalyses, Geophysical Research Letters, 46, 6138–6147, https://doi.org/10.1029/2019GL082781, 2019.

Gregory, J. M., Griffies, S. M., Hughes, C. W., Lowe, J. A., Church, J. A., Fukimori, I., Gomez, N., Kopp, R. E., Landerer, F., Cozannet, G. L., Ponte, R. M., Stammer, D., Tamisiea, M. E., and Van De Wal, R. S. W.: Concepts and Terminology for Sea Level: Mean, Variability and Change, Both Local and Global, Surv Geophys, 40, 1251–1289, https://doi.org/10.1007/s10712-019-09525-z, 2019.

Haigh, I. D., Marcos, M., Talke, S. A., Woodworth, P. L., Hunter, J. R., Hague, B. S., Arns, A., Bradshaw, E., and Thompson, P.: GESLA Version 3: A major update to the global higher-frequency sea-level dataset, Geoscience Data Journal, 10, 293–314, https://doi.org/10.1002/gdj3.174, 2023.

Hinkel, J., Lincke, D., Vafeidis, A. T., Perrette, M., Nicholls, R. J., Tol, R. S. J., Marzeion, B., Fettweis, X., Ionescu, C., and Levermann, A.: Coastal flood damage and adaptation costs under 21st century sea-level rise, Proc. Natl. Acad. Sci. U.S.A., 111, 3292–3297, https://doi.org/10.1073/pnas.1222469111, 2014.

Horsburgh, K. J. and Wilson, C.: Tide-surge interaction and its role in the distribution of surge residuals in the North Sea, J. Geophys. Res., 112, 2006JC004033, https://doi.org/10.1029/2006JC004033, 2007.

Kernkamp, H. W. J., Stelling, G. S., and de Goede, E. D.: Efficient scheme for the shallow water equations on unstructured grids with application to the Continental Shelf, Ocean Dynamics, 2011.

Kirezci, E., Young, I. R., Ranasinghe, R., Muis, S., Nicholls, R. J., Lincke, D., and Hinkel, J.: Projections of global-scale extreme sea levels and resulting episodic coastal flooding over the 21st Century, Sci Rep, 10, 11629, https://doi.org/10.1038/s41598-020-67736-6, 2020.

Knapp, K. R., Kruk, M. C., Levinson, D. H., Diamond, H. J., and Neumann, C. J.: The International Best Track Archive for Climate Stewardship (IBTrACS): Unifying Tropical Cyclone Data, Bull. Amer. Meteor. Soc., 91, 363–376, https://doi.org/10.1175/2009BAMS2755.1, 2010.

Knutson, T., Camargo, S. J., Chan, J. C. L., Emanuel, K., Ho, C.-H., Kossin, J., Mohapatra, M., Satoh, M., Sugi, M., Walsh, K., and Wu, L.: Tropical Cyclones and Climate Change Assessment: Part II: Projected Response to Anthropogenic Warming, Bulletin of the American Meteorological Society, 101, E303–E322, https://doi.org/10.1175/BAMS-D-18-0194.1, 2020.

Kron, W.: Coasts: the high-risk areas of the world, Nat Hazards, 66, 1363–1382, https://doi.org/10.1007/s11069-012-0215-4, 2013.

Lee, J.-W., Irish, J. L., Bensi, M. T., and Marcy, D. C.: Rapid prediction of peak storm surge from tropical cyclone track time series using machine learning, Coastal Engineering, 170, 104024, https://doi.org/10.1016/j.coastaleng.2021.104024, 2021.

Lockwood, J. W., Lin, N., Oppenheimer, M., and Lai, C.: Using Neural Networks to Predict Hurricane Storm Surge and to Assess the Sensitivity of Surge to Storm Characteristics, JGR Atmospheres, https://doi.org/10.1029/2022JD037617, 2022.

Lockwood, J. W., Lin, N., Gori, A., and Oppenheimer, M.: Increasing Flood Hazard Posed by Tropical Cyclone Rapid Intensification in a Changing Climate, Geophysical Research Letters, 51, e2023GL105624, https://doi.org/10.1029/2023GL105624, 2024.

Marcos, M., Wöppelmann, G., Matthews, A., Ponte, R. M., Birol, F., Ardhuin, F., Coco, G., Santamaría-Gómez, A., Ballu, V., Testut, L., Chambers, D., and Stopa, J. E.: Coastal Sea Level and Related Fields from Existing Observing Systems, Surv Geophys, 40, 1293–1317, https://doi.org/10.1007/s10712-019-09513-3, 2019.

Mentaschi, L., Vousdoukas, M. I., García-Sánchez, G., Fernández-Montblanc, T., Roland, A., Voukouvalas, E., Federico, I., Abdolali, A., Zhang, Y. J., and Feyen, L.: A global unstructured, coupled, high-resolution hindcast of waves and storm surge, Front. Mar. Sci., 10, 1233679, https://doi.org/10.3389/fmars.2023.1233679, 2023.

Merkens, J.-L., Reimann, L., Hinkel, J., and Vafeidis, A. T.: Gridded population projections for the coastal zone under the Shared Socioeconomic Pathways, Global and Planetary Change, 145, 57–66, https://doi.org/10.1016/j.gloplacha.2016.08.009, 2016.

Muis, S., Verlaan, M., Winsemius, H. C., Aerts, J. C. J. H., and Ward, P. J.: A global reanalysis of storm surges and extreme sea levels, Nat Commun, 7, 11969, https://doi.org/10.1038/ncomms11969, 2016.

Muis, S., Lin, N., Verlaan, M., Winsemius, H. C., Ward, P. J., and Aerts, J. C. J. H.: Spatiotemporal patterns of extreme sea levels along the western North-Atlantic coasts, Sci Rep, 9, 3391, https://doi.org/10.1038/s41598-019-40157-w, 2019.

Muis, S., Apecechea, M. I., Dullaart, J., de Lima Rego, J., Madsen, K. S., Su, J., Yan, K., and Verlaan, M.: A High-Resolution Global Dataset of Extreme Sea Levels, Tides, and Storm Surges, Including Future Projections, Front. Mar. Sci., 7, 263, https://doi.org/10.3389/fmars.2020.00263, 2020.

Muis, S., Aerts, J. C. J. H., Á. Antolínez, J. A., Dullaart, J. C., Duong, T. M., Erikson, L., Haarsma, R. J., Apecechea, M. I., Mengel, M., Le Bars, D., O'Neill, A., Ranasinghe, R., Roberts, M. J., Verlaan, M., Ward, P. J., and Yan, K.: Global Projections of Storm Surges Using High-Resolution CMIP6 Climate Models, Earth's Future, 11, e2023EF003479, https://doi.org/10.1029/2023EF003479, 2023.

Nearing, G., Cohen, D., Dube, V., Gauch, M., Gilon, O., Harrigan, S., Hassidim, A., Klotz, D., Kratzert, F., Metzger, A., Nevo, S., Pappenberger, F., Prudhomme, C., Shalev, G., Shenzis, S., Tekalign, T. Y., Weitzner, D., and Matias, Y.: Global prediction of extreme floods in ungauged watersheds, Nature, 627, 559–563, https://doi.org/10.1038/s41586-024-07145-1, 2024.

Nevo, S., Morin, E., Gerzi Rosenthal, A., Metzger, A., Barshai, C., Weitzner, D., Voloshin, D., Kratzert, F., Elidan, G., Dror, G., Begelman, G., Nearing, G., Shalev, G., Noga, H., Shavitt, I., Yuklea, L., Royz, M., Giladi, N., Peled Levi, N., Reich, O., Gilon, O., Maor, R., Timnat, S., Shechter, T., Anisimov, V., Gigi, Y., Levin, Y., Moshe, Z., Ben-Haim, Z., Hassidim, A., and Matias, Y.: Flood forecasting with machine learning models in an operational framework, Hydrol. Earth Syst. Sci., 26, 4013–4032, https://doi.org/10.5194/hess-26-4013-2022, 2022.

Palmer, M. D., Domingues, C. M., Slangen, A. B. A., and Boeira Dias, F.: An ensemble approach to quantify global mean sea-level rise over the 20th century from tide gauge reconstructions, Environ. Res. Lett., 16, 044043, https://doi.org/10.1088/1748-9326/abdaec, 2021.

Parker, K., Erikson, L., Thomas, J., Nederhoff, K., Barnard, P., and Muis, S.: Relative contributions of water-level components to extreme water levels along the US Southeast Atlantic Coast from a regional-scale water-level hindcast, Nat Hazards, https://doi.org/10.1007/s11069-023-05939-6, 2023.

Pörtner, H.-O., Roberts, D. C., and Masson-Delmotte, V.: The Ocean and Cryosphere in a Changing Climate: Special Report of the Intergovernmental Panel on Climate Change, Cambridge University Press, https://doi.org/10.1017/9781009157964, 2022.

Resio, D. T. and Westerink, J. J.: Modeling the physics of storm surges, Physics Today, 61, 33–38, https://doi.org/10.1063/1.2982120, 2008.

Soci, C., Hersbach, H., Simmons, A., Poli, P., Bell, B., Berrisford, P., Horányi, A., Muñoz-Sabater, J., Nicolas, J., Radu, R., Schepers, D., Villaume, S., Haimberger, L., Woollen, J., Buontempo, C., and Thépaut, J.: The ERA5 global reanalysis from 1940 to 2022, Quart J Royal Meteoro Soc, qj.4803, https://doi.org/10.1002/qj.4803, 2024.

Tadesse, M., Wahl, T., and Cid, A.: Data-Driven Modeling of Global Storm Surges, Front. Mar. Sci., 7, 260, https://doi.org/10.3389/fmars.2020.00260, 2020.

Tadesse, M. G. and Wahl, T.: A database of global storm surge reconstructions, Sci Data, 8, 125, https://doi.org/10.1038/s41597-021-00906-x, 2021.

Tiggeloven, T., Couasnon, A., van Straaten, C., Muis, S., and Ward, P. J.: Exploring deep learning capabilities for surge predictions in coastal areas, Sci Rep, 11, 17224, https://doi.org/10.1038/s41598-021-96674-0, 2021.

Wessel, P. and Smith, W. H. F.: A global, self-consistent, hierarchical, high-resolution shoreline database, J. Geophys. Res., 101, 8741–8743, https://doi.org/10.1029/96JB00104, 1996.

Woodworth, P. L., Melet, A., Marcos, M., Ray, R. D., Wöppelmann, G., Sasaki, Y. N., Cirano, M., Hibbert, A., Huthnance, J. M., Monserrat, S., and Merrifield, M. A.: Forcing Factors Affecting Sea Level Changes at the Coast, Surv Geophys, 40, 1351–1397, https://doi.org/10.1007/s10712-019-09531-1, 2019.

Xiong, J.: Evaluation and improvement of the ERA5 wind field in typhoon storm surge simulations, Applied Ocean Research, 2022.

Yang, L., Jin, T., Xiao, M., Gao, X., Jiang, W., and Li, J.: Extreme Events and Probability Analysis Along the United States East Coast Based on High Spatial-Coverage Reconstructed Storm Surges, Geophysical Research Letters, 50, e2023GL103492, https://doi.org/10.1029/2023GL103492, 2023.

Yang, L., Jin, T., and Jiang, W.: ASM-SS: The First Quasi-Global High Spatial Resolution Coastal Storm Surge Dataset Reconstructed from Tide Gauge Records [data set], https://doi.org/10.5281/zenodo.14034726, 2024a.

Yang, L., Jin, T., and Jiang, W.: Improving Coastal Storm Surge Monitoring Through Joint Modeling Based on Permanent and Temporary Tide Gauges, Geophysical Research Letters, 51, e2024GL108886, https://doi.org/10.1029/2024GL108886, 2024b.